PHOTOMASK

BACUS—The international technical group of SPIE dedicated to the advancement of photomask technology.

2014 Karel Urbanek Best Student Paper Award

# Determination of line edge roughness in low dose top-down scanning electron microscopy images

**T. Verduin, P. Kruit, and C.W. Hagen,** Delft University of Technology, Faculty of Applied Sciences, Department of Imaging Physics, Lorentzweg 1, 2628 CJ Delft, The Netherlands

## ABSTRACT

We investigated off-line metrology for LER determination in low-dose SEM images to reduce the acquisition time and the risk of shrinkage. Our first attempts are based on filtering noisy (experimental) SEM images and use peak detection to measure the edge displacements and calculating the discrete PSD. However, the result of the filtering is that the power spectrum of the filter leaks into the PSD. So it is better to avoid a filter at all. We subsequently developed a method to detect edge displacements without the use of a filter. This method considers the signal profile of a SEM by integrating an experimental image of lines in the direction of the edges. The signal profile of an isolated edge is modeled as two merged Gaussians. This signal profile is then fitted against the raw (unfiltered) data of the edge pattern using an interior trust-region-reflective minimization procedure. This gives the edge displacements without the use of a filter and a filter-free version of the discrete PSD is obtained. The determination of edge displacements without the use of a filter, enables us to study how much noise is acceptable and still determine LER. To answer this question we generate random lines using the model of Palasantzas and the algorithm of Thorsos.

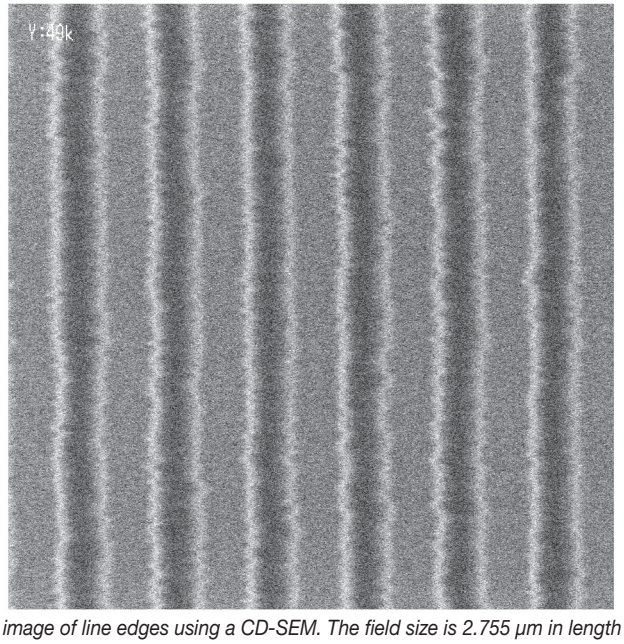


*Figure 1. Recorded image of line edges using a CD-SEM. The field size is 2.755 µm in length (1024 pixels) and 450 nm wide (1024 pixels). The pixel size is approximately 2.7 nm x 0.4 nm.*

BACUS NEWS

MAY 2014
VOLUME 30, ISSUE 5

TAKE A LOOK INSIDE:



SPIE.

9050-20

# EDITORIAL

## Slow, Steady . . . EUV

**Wilbert Odisho,** KLA-Tencor Corporation

Everyone is closely monitoring industry progress on the next-generation lithography solutions that leading chip manufacturers are exploring. While KLA-Tencor is not in the position to conduct its own investigation of possible advanced patterning solutions, we believe EUV lithography (EUVL) is the most direct path for patterning below the 10nm design node. It's a bumpy path, with every two steps forward being met with a step backwards, but forward progress is being made and the momentum towards implementing EUVL is unstoppable. Additional patterning technologies, such as Directed Self-Assembly (DSA), e-beam direct write, and 193i multi-patterning techniques are also being actively explored by IC manufacturers, and going forward, they may choose one or more of these alternate patterning paths. Our role is to enable process control and fast yield ramps as chipmakers travel along any of these routes, and as such, we have comprehensive inspection and metrology roadmaps to support this diverse range of advanced patterning solutions.

Our road to supporting EUVL began in 2008, when we gathered scientists and researchers from around the world to form a team focused on EUV Actinic Patterned and Blank Mask Inspection (APMI) technology development. We call this the 710 program – the seventh generation mask inspection platform in the Reticle and Photomask Product Division (RAPID). It is the largest platform program in our history – large in so many aspects, from physical size, costs and technical challenges to resulting innovations, engineering talent and collaborations. The 710 program's objective is to enable at-wavelength mask defect detection and disposition to support EUV lithography in the high volume manufacturing (HVM) environment.

The industry has lived through EUVL HVM insertion timing uncertainty for a number of years now, and as we move along this road with an elusive finish line, we're seeing new requirements on the horizon – such as a pellicle for the EUV mask, higher NA scanner optics and its requirements for mask size and magnification. We expect key EUVL technology suppliers will not stop or slow down their efforts to close the gaps on EUVL production readiness. We are not an exception. We must stay on track to meet our key customers' needs. Our 193nm-based mask inspection platform, the Teron 630 Series, provides inspection capability for both blank and patterned EUV masks which we believe will meet near-term pilot production defectivity learning requirements. In the meantime, we continue collaborating with our strategic partners and suppliers through periodic technical and business exchanges to jointly address new challenges and identify promising opportunities in relation to enabling technologies and cost management. We and our customers believe Actinic Patterned Mask Inspection technology is necessary for success in EUV lithography, especially since it is the only solution for through-pellicle inspection.

One key challenge we face is the magnitude of the investment we need to make to support our next-generation patterning defect control solution for reticles. We firmly believe this investment is important, even though the total available market size for this platform will likely be small. We have formed a Product Readiness Partnership program with key customers focusing on concept and feasibility investigations and have successfully developed a viable system architecture. Moving forward, we are collaborating with our customers even more closely to further reduce business and technical risks.

What's next? We are continuing along our APMI path, moving forward with our concept development and risk reduction activities. Significant effort has been spent on achieving ultra-clean vacuum levels to protect optics from contamination in order to have a production-worthy APMI system. We now have the latest-generation EUV light source installed on a new chamber and testing is in progress. Our in-house vacuum particle test fixture has identified particle generation sources, helping our engineers to substantially improve particle per reticle pass performance. In addition, we are constantly seeking ways to manage the costs more effectively, as it is the fact that APMI development poses a large financial challenge. Overall, through our customer collaborations and engineering innovations, we expect our APMI technology path will merge with EUVL when it's ready to make the step forward into production.

BACUS

N • E • W • S

*BACUS News* is published monthly by SPIE for BACUS, the international technical group of SPIE dedicated to the advancement of photomask technology.

**Managing Editor/Graphics** Linda DeLano
**Advertising** Lara Miles
**BACUS Technical Group Manager** Pat Wight

■ 2014 BACUS Steering Committee ■

**President**
Frank E. Abboud, *Intel Corp.*

**Vice-President**
Paul W. Ackmann, *GLOBALFOUNDRIES Inc.*

**Secretary**
Bryan S. Kasprowicz, *Photronics, Inc.*

**Newsletter Editor**
Artur Balasinski, *Cypress Semiconductor Corp.*

**2014 Annual Photomask Conference Chairs**
Paul W. Ackmann, *GLOBALFOUNDRIES Inc.*
Naoya Hayashi, *Dai Nippon Printing Co., Ltd.*

**International Chair**
Uwe F. W. Behringer, *UBC Microelectronics*

**Education Chair**
Artur Balasinski, *Cypress Semiconductor Corp.*

**Members at Large**
Paul C. Allen, *Toppan Photomasks, Inc.*
Michael D. Archuletta, *RAVE LLC*
Peter D. Buck, *Mentor Graphics Corp.*
Brian Cha, *Samsung*
Glenn R. Dickey, *Shin-Etsu MicroSi, Inc.*
Brian J. Grenon, *Grenon Consulting*
Thomas B. Faure, *IBM Corp.*
Jon Haines, *Micron Technology Inc.*
Mark T. Jee, *HOYA Corp, USA*
Oliver Kienzle, *Carl Zeiss SMS GmbH*
Patrick M. Martin, *Applied Materials, Inc.*
M. Warren Montgomery, *The College of Nanoscale Science and Engineering (CNSE)*
Wilbert Odisho, *KLA-Tencor Corp.*
Abbas Rastegar, *SEMATECH North*
Emmanuel Rausa, *Plasma-Therm LLC.*
Douglas J. Resnick, *Molecular Imprints, Inc.*
Thomas Struck, *Infineon Technologies AG*
Bala Thumma, *Synopsys, Inc.*
Jacek K. Tyminski, *Nikon Precision Inc.*
Larry S. Zurbrick, *Agilent Technologies, Inc.*

SPIE.

P.O. Box 10, Bellingham, WA 98227-0010 USA
Tel: +1 360 676 3290
Fax: +1 360 647 1445
www.SPIE.org
help@spie.org

©2014

All rights reserved.

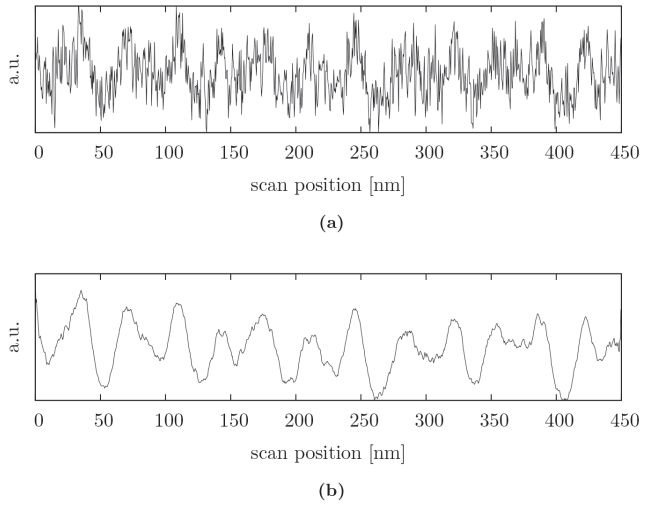


*Figure 2. Amplitude of a single horizontal scan-line taken from the center of figure 1. The top figure is the raw (unfiltered) signal. This signal is too noisy for edge detection, therefore a Gaussian filter is applied (bottom figure).*

This gives random generated edge displacements for typical values of experimental lines for the parameters of the model: 2 µm long lines (256 pixels), a correlation length ε of 25 nm and a roughness exponent α of 0.75. A noise-free top-down SEM-like image of lines is created by shifting the profile signal according to the random generated edge displacements. The image is further processed by adding Poisson-distributed noise. We consider three noise cases where the average electron density is about 2, 20 and 200 electrons per pixel. This corresponds to a charge density of (in respective order) 10 µC/cm$^2$, 100 µC/cm$^2$ and 1000 µC/cm$^2$. The edge displacements of the random generated images are determined using our new developed filter-free displacement detection. The difference between the random generated displacements and the detected displacements (after adding Poisson-distributed noise) shows how pixel noise translates to noise in edge displacements. We conclude from running many simulations that this pixel noise translates to a noise in the edge displacements which is uniform (flat line) in the PSD. This means that pixel noise is classified as white noise in the edge displacements. Finally, we study simulated discrete PSDs as a function of the number of averages and analyze the convergence of the parameters ($\sigma$, $\sigma_n$, $\varepsilon$ and $\alpha$) of the Palasantzas model extended with a white noise term. One of the conclusions is that a very noisy image with 12 lines and about 2 electrons per pixel on average (charge density ≈ 10 µC/cm$^2$) already produces an estimation for LER with a relative error of about 10%.

## 1. Introduction

The determination of Line Edge Roughness (LER) and Line Width Roughness (LWR) becomes increasingly important as the semiconductor devices decrease in dimensions[1,2,3]. This results in smaller tolerances on LER/LWR and as a consequence, the metrology becomes more critical.

There are two classes of LER metrology. There is on-line metrology, which is typically performed in SEMs combined with

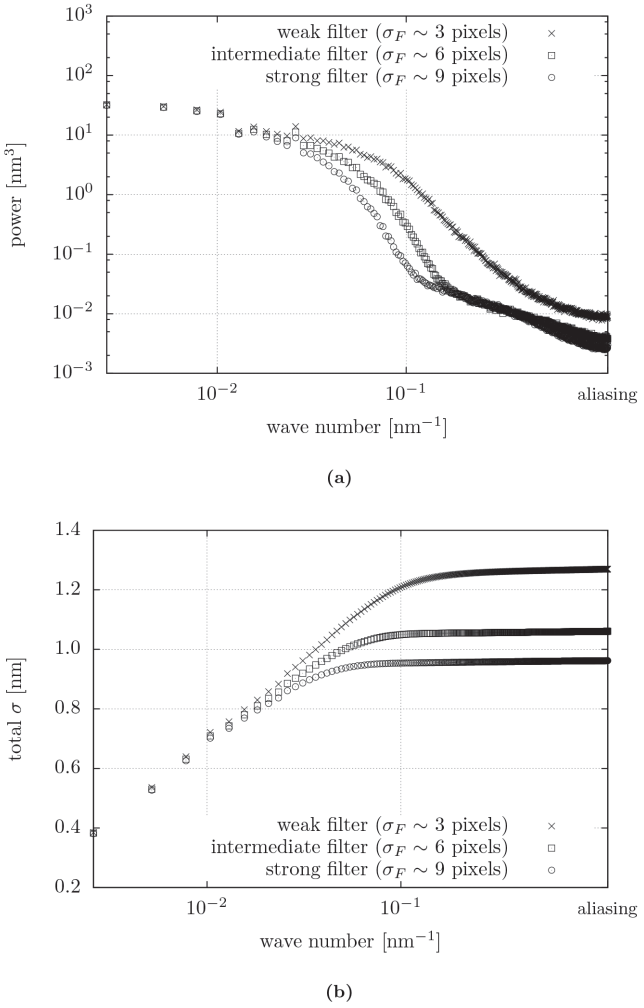


*Figure 3. This image shows the calculated discrete PSD obtained from analyzing the set of images from J. Jussot (see figure 1). The markers correspond to different strengths of the symmetric two- dimensional Gaussian filter. The bottom figure shows the cumulative sum, which gives the total σ via Parseval's relation given by equation 4. Note that the total σ becomes a function of the filter.*

dedicated (proprietary) software for LER analysis. Another class is off-line metrology and only deals with the image analysis. The latter is used for instance for resist characterization. Examples of off-line metrology are described by[4,5,6,7]. Typically in LER analysis, the fluctuations in edge displacements are determined by using a Canny-edge detection filter or by a homemade edge detection algorithm, see for example[4]. Although the edge displacements are already a direct measurement of the roughness, LER is best analyzed by the Power Spectral Density (PSD). There are a couple of problems related to this type of determination. First of all, there are statistical and systematic errors because the actual PSD is approximated by sampling the edge displacements of a pattern with a finite number of measurement intervals. The statistical errors are described by[8]. The systematic errors have recently been studied by[9]. There is also the problem of shrinkage, where the act of measuring

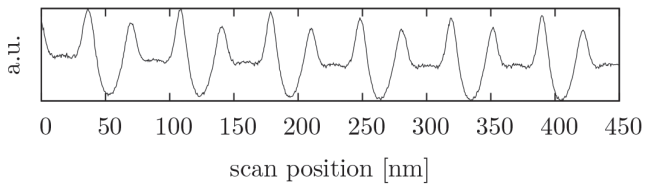


*Figure 4. Image of approximated SEM signal profile. This profile is obtained by integrating figure 1 in the direction of the edges.*

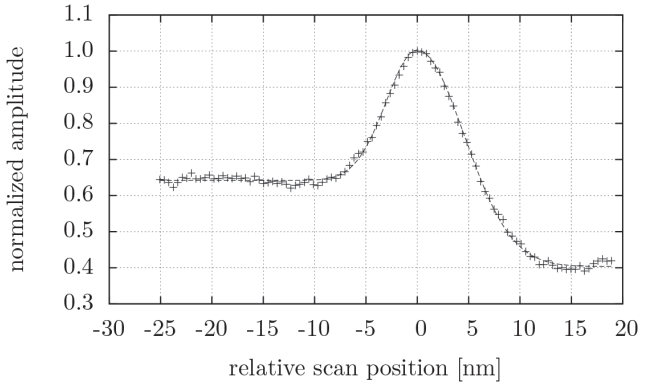


*Figure 5. Illustration of the signal profile of an isolated edge of figure 4.*

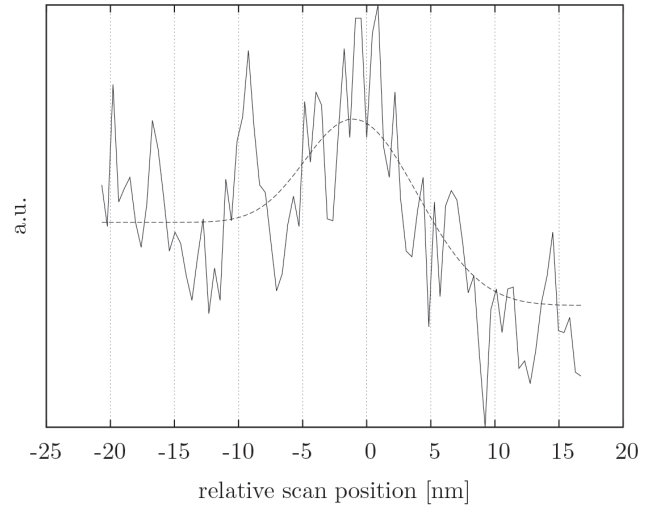


*Figure 6. Illustration of minimizing the model for the signal profile in the unfiltered data by varying the horizontal displacement and vertical scale of the merged Gaussians.*

the edge displacements by irradiating with an e-beam induces changes in the pattern, see for example[5,7,10]. Finally, it takes a long time to obtain good low-noise images, which are now required for edge detection. In this article we focus on off-line metrology and investigate how much noise is acceptable by decreasing the dose in simulated top-down SEM-like images

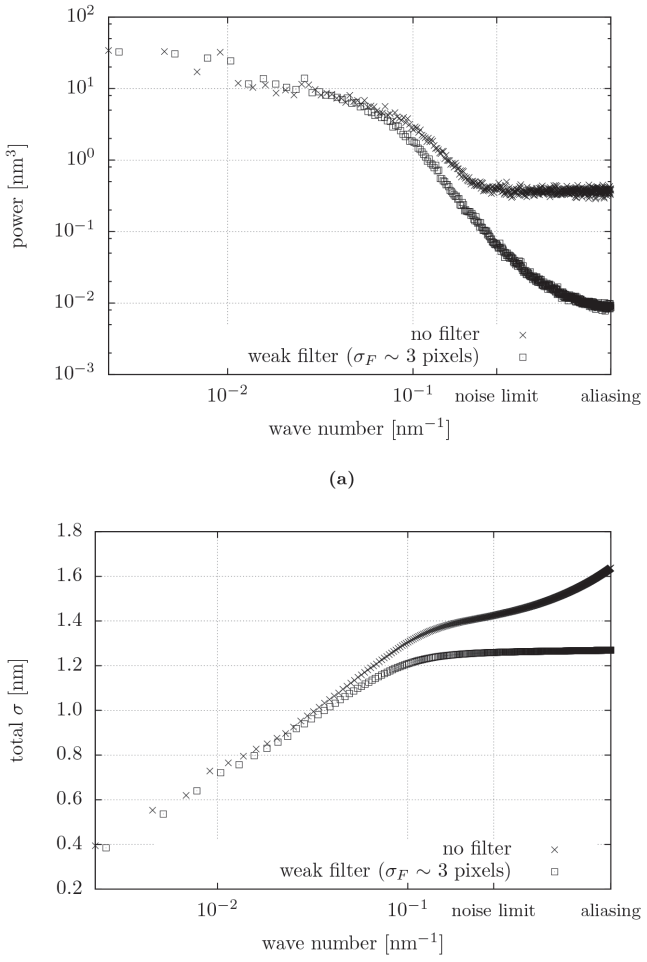


*Figure 7. This image shows the calculated discrete PSD obtained from analyzing the set of images from J. Jussot (see figure 1). The square markers correspond to the weakest filter of figure 3a. This figure also includes the discrete PSD obtained by fitting the profile signal against the experimental image. The bottom figure shows the cumulative sum, which gives the total σ via Parseval's relation (equation 4).*

and analyze how many images of the edges are required for estimating LER-related parameters.

## 2. Line Edge Determination

An example of a top-down SEM image of line edges is given in figure 1, which was recorded by J. Jussot from CNRS-LTM/CEA-LETI in 2012. The properties of the resist are unknown to us due to disclosure restrictions. In figure 2a we illustrate the amplitude of a single horizontal scan-line taken from the center row of image 1. Peak based detection algorithms, such as the Canny-edge detector, often do not find the edge or find too many edges in such noisy data. Working with low-noise images has two problems: (1) They take a long time to accumulate and (2) there is a risk of resist shrinkage. An obvious way to reduce the noise is to apply a filter to the recorded image. By applying a filter we reduce the noise in the signal, which is illustrated

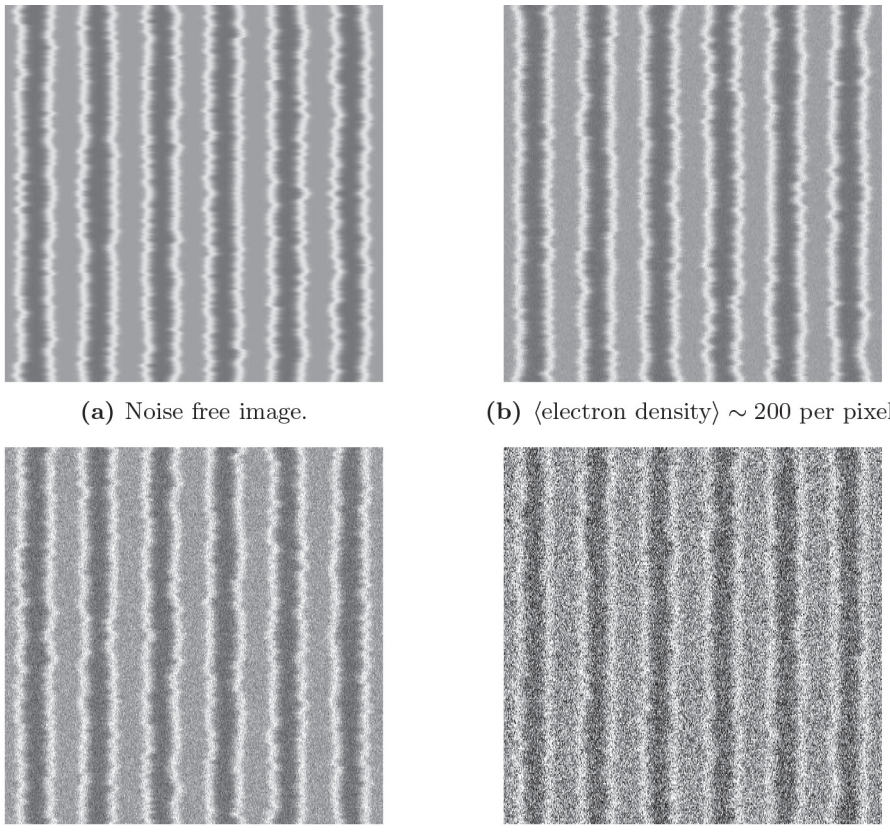

**(a)** Noise free image.

**(b)** ⟨electron density⟩ ∼ 200 per pixel.

**(c)** ⟨electron density⟩ ∼ 20 per pixel.

**(d)** ⟨electron density⟩ ∼ 2 per pixel.

*Figure 8. Random generated top-down SEM-like image with line edges. The field size is 2 µm in length (256 pixels) and 450 nm wide (1024 pixels). The pixel size is about 7 nm x 0.5 nm.*

in figure 2b. At this point edge detection is possible and the edge displacements along the line are measured.

The discrete PSD of the edge displacements is obtained by calculating the amplitude of the Fourier coefficients,

$$P_n = \frac{L}{2\pi} |F_n|^2 \qquad (1)$$

Where the discrete Fourier transform is determined as,

$$F_n = \frac{1}{N} \sum_{j=0}^{N-1} (x_j - \langle x \rangle_N) \exp(-ik_n j \Delta y) \qquad (2)$$

Where $N$ is the number of sampled edge displacements, $x_j$ the displacement of the $j^{th}$ edge position, $(x)_N$ the mean position of the edge, $\Delta y$ the measurement interval and $k_n$ the discrete wavenumber i.e.,

$$k_n = \frac{2\pi n}{L} \qquad (3)$$

Where $n$ = 0, 1, 2, . . . ,$N$ – 1 and $L$ the length of the edge. The following identity relates the variance of the edge displacements to the PSD,

$$\sigma^2 = \frac{2\pi}{L} \sum_{n=0}^{N-1} P_n \qquad (4)$$

Which is Parseval's relation. The discrete PSD given by equation 1 is only an approximation to the actual spectrum of a quasi-infinite long line and the finite edge length $L$ is a source of statistical noise, see for example[8]. The statistical noise in the discrete PSD is reduced by averaging over many lines,

$$P_n = \frac{L}{2\pi} \left\langle |F_n|^2 \right\rangle_{N^\star} \qquad (5)$$

Where $N^*$ counts the number of lines over which the PSD is averaged.

We calculated the discrete PSD of the edges illustrated in figure 1 by using about 50 different recorded images of line edges of the same kind. Each image is at first processed with a symmetric two-dimensional Gaussian filter with strength $\sigma_F$. The edge displacements are then measured using a homemade edge detection algorithm. The results of using filter strength $\sigma_F \approx 3$ pixels (cross markers), $\sigma_F \approx 6$ pixels (square markers) and $\sigma_F \approx 9$ pixels (circular markers) are given in figure 3a. In figure 3b we plot the square root of the cumulative sum of the PSD from the lowest wave number towards the higher wave numbers. This cumulative sum gives the variance via Parseval's relation (equation 4) and by taking the square root we can see how the standard deviation develops as a function of wave number. The cross markers in figures 3a and 3b correspond to the weakest filter that we could apply such that every scan-line in the SEM image (see for example figure 1) produces the correct number

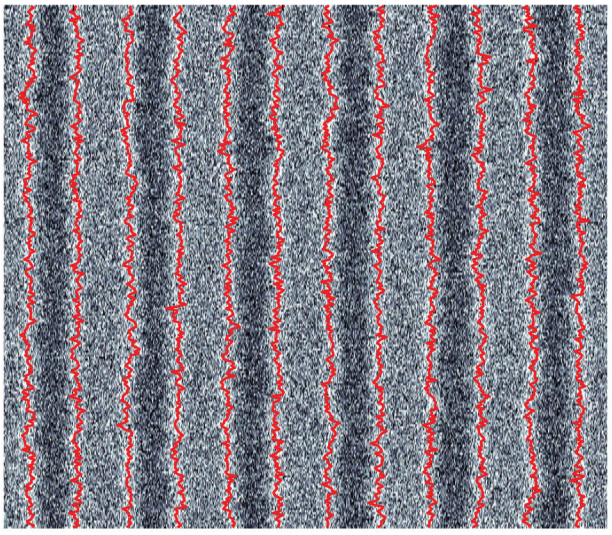

*Figure 9. Illustration of filter-free displacement detection applied to a random generated top-down SEM-like image with lines. The field size is 2 µm in length (256 pixels) and 450 nm wide (1024 pixels). The average electron density of this image is about 2 electrons per pixel and corresponds to an average charge density of about 10 µC/cm².*

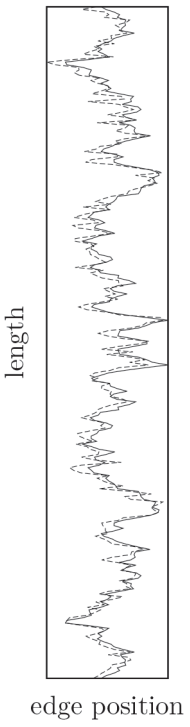


*Figure 10. Illustrative comparison between the random generated displacements (solid line) and the detected displacements (dashed line) after adding Poisson-distributed noise. The difference between the input and detected displacements gives us the noise distribution in edge detection caused by adding pixel noise.*

of edges (12). In other words, if we decrease the strength of the filter even further, then we no longer detect 12 edges per scan-line. In figure 3a we observe that, besides suppression of the high frequencies (which is required to reduce the image noise), the lower and center frequencies are affected as well. The conclusion from figure 3a is that the power spectrum of the filter leaks into the PSD. As a consequence, LER becomes a function of the applied filter, which is best seen in figure 3b. We ask the following question: How much further do we need to reduce the filter strength, such that the measured LER no longer depends on the filter? We failed in reducing the strength of the filter because then the edges cannot be detected accurately anymore by conventional peak detection. The side effect of image processing, in particular smoothing, is also discussed by[4, 11]. Now that we see the influence of a filter on the PSD, we conclude that the best solution would be to avoid a filter at all.

We recently developed a method to detect edge displacements without the use of a filter. This method works as follows. We approximate the signal profile of the SEM by integrating the image in the direction of the edges. For example, the approximate signal profile of figure 1 is given by figure 4. We emphasize that this is only an approximation, because by integrating in the direction of the edges, the actual shape of this profile becomes a function of the roughness of the edges. We expect that if the roughness increases, then the signal profile widens. In principle, the roughness of the edges must be corrected for by displacing the rows. However, for the moment we assume that this roughness dependency can be neglected. The signal profile of a single edge is shown in figure 5. We model this signal profile by matching two vertically shifted and normalized Gaussians at the center of the peak, which has the following mathematical representation,

$$P(x) = \begin{cases} b_L + (1 - b_L) \exp\left(-\frac{1}{2}\frac{(x-\mu)^2}{\sigma_L^2}\right) & x < \mu \\ b_R + (1 - b_R) \exp\left(-\frac{1}{2}\frac{(x-\mu)^2}{\sigma_R^2}\right) & x \geq \mu \end{cases} \quad (6)$$

Where $b_L$ and $b_R$ defines the base level, $\sigma_L$ and $\sigma_R$ define the standard deviation to the left and right of the center $\mu$.

The left base level is defined such that $\lim_{x \to +[x]} P(x) = b_L$ and the right base is defined such that $\lim_{x \to +[x]} P(x) = b_R$. Note that if $b_L = b_R = 0$ (the Gaussians are not shifted upwards), and $\sigma_L = \sigma_R$ (same spread), then equation 6 reduces to the standard definition of a Gaussian distribution (neglecting the normalization factor). The parameters $b_L$, $b_R$, $\sigma_L$ and $\sigma_R$ are fitted against the approximated signal profile. The dashed line in figure 5 is the best fit of this model against a single isolated experimental profile obtained by integrating image 1 in the direction of the edge. The idea is now to fit this model to every sampled row of a single edge using parameter optimization. We introduce the following degrees of freedom to the model of the fitted signal profile,

$$s \cdot P(x - \Delta x) \quad (7)$$

Where $s$ scales the profile vertically and $\Delta x$ is the horizontal displacement of the profile. The parameters $s$ and $\Delta x$ are determined by using an interior trust-region-reflective minimization algorithm. The interested reader is referred to the article of Coleman for details on the minimization procedure[12]. In figure 6 we demonstrate one of the minimization results using the original (unfiltered) signal. Clearly for such noisy data, an edge detection method could not have found the position of the edge.

Now that we can detect the edge displacements without using a filter, we re-analyze the recorded images of J. Jussot (figure 1). The PSD without using a filter (cross markers) is given by figure 7a together with the weak filter version (square

BACUS NEWS

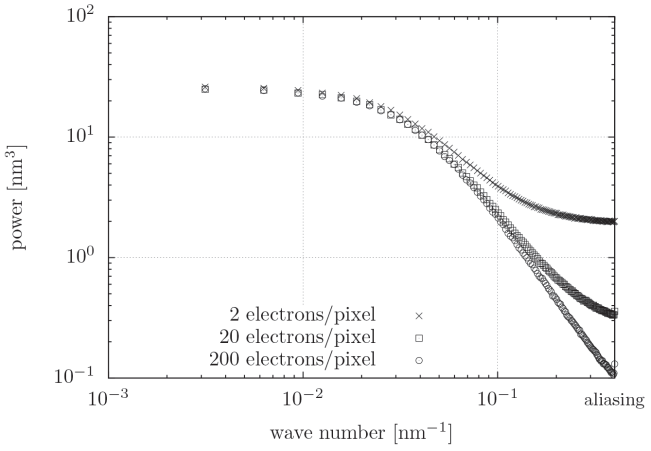


*Figure 11. Simulated PSD obtained from averaging over many images for different noise settings.*

markers) of figure 3a. In figure 7a we can see that the pixel noise really starts to contribute after the marker 'noise limit'. In figure 7b we see that the cumulative sum after the marker accounts for approximately 1.6nm - 1.4nm = 0.2nm. Therefore, a rough estimation for the actual LER is 1.4nm. This is to be compared to the estimate of 1.3nm for the weak filter version (square markers) in figure 7b. Apparently, the weakest filter that we have applied before is not that far off.

## 3. Image Noise Analysis

In estimating LER (figure 7a) we used all available images (+50) to reduce the uncertainty in the discrete PSD. We now improved this LER determination by considering a model for the PSD and question how much noise is acceptable, such that we still can determine LER? In fact there are two questions: (1) How much noise can we allow in a single image and (2) how many lines/images do we need in total? We begin our investigation on the effect of image noise on the determination of LER by generating rough edges at random using the model of Palasantzas[13] with known parameters,

$$\mathrm{PSD}(k) = \frac{\sqrt{\pi}}{2\pi}\frac{\Gamma\left(\alpha+\frac{1}{2}\right)}{\Gamma(\alpha)}\frac{2\sigma^2\xi}{\left(1+k^2\xi^2\right)^{\alpha+\frac{1}{2}}} \qquad (8)$$

This PSD defines a perfect infinitely long line with $\sigma$ as the LER, $\varepsilon$ the correlation length and $\alpha$ the roughness exponent. It can be verified that this PSD satisfies the following identity,

$$\sigma^2 = \int_{-\infty}^{+\infty} \mathrm{PSD}(k)\,\mathrm{d}k \qquad (9)$$

The random displacements can be generated via the algorithm of Thorsos, which is explained in[14]. The algorithm of Thorsos produces random edge displacements that, in the limit of large averages, converges towards the PSD of Palasantzas up to a bias in the standard deviation. This bias is explained in[14] as well and can be compensated for by multiplying the edge displacements with a constant factor.

We generate top-down SEM-like images by using the fitted signal profile obtained earlier (figure 5). A SEM-like image is obtained by shifting the signal profile at every row according to

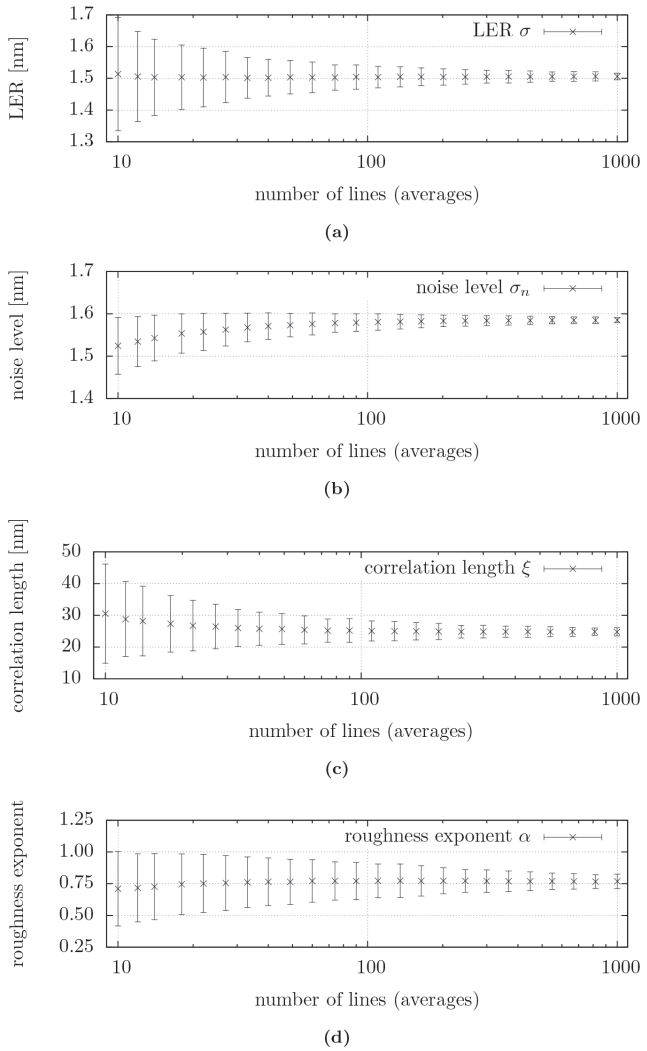


*Figure 12. Simulation results for fitting the PSD model of Palasantzas to random generated lines after adding Poisson-distributed noise. The random lines are generated with a length of 2 µm (256 pixels) using the fitted signal profile of figure 5. The correlation length ε is set to 25 nm and the roughness exponent α equals 0.75. The simulated (electron density) ~ 2 per pixel (charge density ≈ 10 µC/cm²).*

the random generated displacements satisfying equation 8. If we put a number of random generated lines next to each other in one image, we obtain the result of figure 8a. This is a simulated result of a noise-free top-down SEM-like image of random generated line edges. The image is further processed by adding Poisson-distributed noise to every pixel of the noise-free image, after choosing an average electron density. Examples of Poisson noise generated images are given by figures 8b, 8c and 8d. In each of the images, the average electron density is set to (in respective order): 200, 20 and 2 electrons per pixel. The corresponding average charge density is (in respective order): 1000 µC/cm², 100 µC/cm² and 10 µC/cm². The edges of the random generated images are determined using filter-free displacement detection as described before. An example of displacement detection applied to a random generated im-

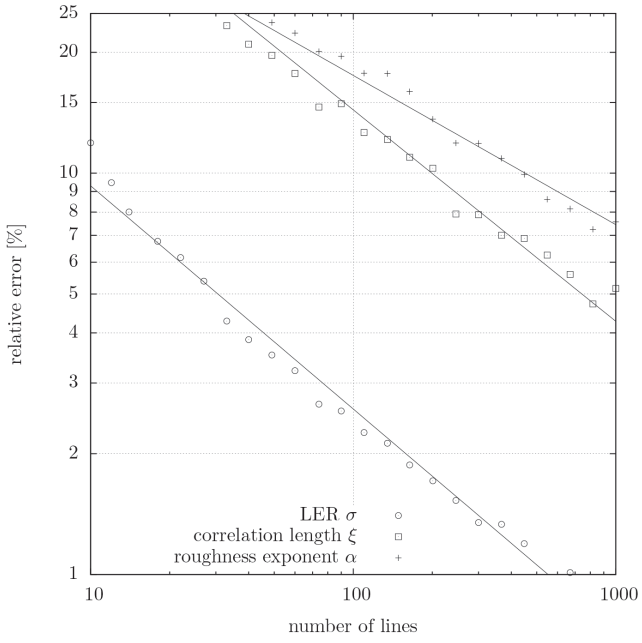


*Figure 13. Relative error in parameter estimation in the simulation of figure 12. This result corresponds to an average density of 2 electrons per pixel.*

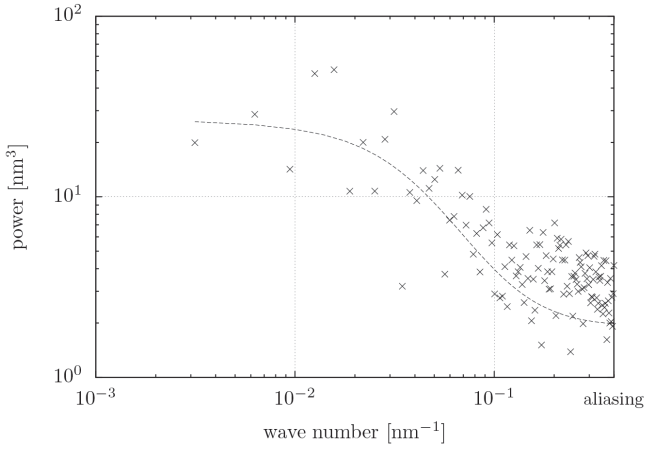


*Figure 14. Illustration of the intrinsic noise in the discrete PSD after averaging 10 times. The dashed line corresponds to the limit of many averages. The data is obtained from a simulation corresponding to a density of about 2 electrons per pixel (charge density ≈ 10 μC/cm²).*

age is given by figure 9. The difference between the random generated displacements and the detected displacements after adding Poisson-distributed noise tells us how pixel noise translates to noise in edge displacements. This is illustrated in figure 10, where the black line corresponds to the random generated displacements and the dashed line corresponds to the detected displacements after adding Poisson-distributed noise. We conclude from running many simulations that this pixel noise translates to a noise in the edge displacements which is uniform (flat line) in the PSD. This means that pixel noise is classified as white noise in the edge displacements. Now that we classified the noise, we are free to add this noise term to the Palasantzas model (see also[7, 9]),

$$\mathrm{PSD}_{\mathrm{w/noise}}(k) = \mathrm{PSD}_{\mathrm{w/o\ noise}}(k) + \sigma_n^2 \frac{\Delta y}{2\pi} \qquad (10)$$

Where $\sigma_n$ is the noise level and $\Delta y$ the measurement interval. The PSDs obtained by detecting the edge displacements in simulated images with an electron density of 2, 20 and 200 electrons per pixel are given by figure 11. In these images we can see that pixel noise translates to white noise: The PSD in the high frequencies flattens out to a straight line as we increase the noise level by decreasing the electron density per pixel.

The idea is now to fit the simulated discrete PSD as a function of the number of averages and analyze the convergence of the parameters ($\sigma$, $\sigma_n$, $\varepsilon$ and $\alpha$) of the Palasantzas model extended with a noise term, see equation 10. We remark that by fitting equation 10, we neglect the systematic errors described by[9]. We neglect the systematic errors because we have a larger *N* and the power of the noise level renders the perturbation due to aliasing or spectral leakage negligible. Our simulation is set up as follows: We generate random lines with a length of 2 μm (256 pixels) using the fitted signal profile of figure 5. The correlation length $\varepsilon$ in the Palasantzas model is set to 25 nm and the roughness exponent $\alpha$ equals 0.75. These are typical values for experimentally measured edges[7, 9]. Now we consider the worst case in image noise of the densities given by figure 8, which corresponds to an electron density of about 2 electrons per pixel on average (charge density ≈ 10 μC/cm²). We run many simulations and determine distributions of the outcome values of the parameters of the Palasantzas model (LER $\sigma$, noise level $\sigma_n$, correlation length $\varepsilon$ and roughness exponent $\alpha$). The result of this low dose high-noise simulation is given by figure 12. At first we observe that all estimated parameters of the Palasantzas model are likely to converge towards the input parameters. However, the convergence seems to be asymptotic, which is best seen in the noise term $\sigma_n$ (figure 12b) and correlation length $\varepsilon$ (figure 12c). The errorbars roughly decrease as the square root of the number of averages, which is to be expected based on averaging principles. The relative errors (size of the errorbars divided by the input value of the parameter) are given in figure 13. We conclude from figure 13 that the correlation length $\varepsilon$ and roughness exponent $\alpha$ are harder to estimate, i.e. it takes more averages to produce the same relative error as for LER $\sigma$ and noise level $\sigma_n$. The most interesting parameter for industry is LER $\sigma$, because that is the parameter against which process performance is evaluated. When the number of averages is low, the intrinsic noise in the discrete PSD is significant, as can be seen in figure 14. It is remarkable that under these conditions LER can still be estimated with a relative error of about 10%. In other words, it only takes one single image (figure 8d) with 2 electrons per pixel (charge density ≈ 10 μC/cm²) to estimate LER as 1.5 nm ± 10%.

We now question how the parameters converge when we change to a different electron density per pixel. The influence of electron density on LER $\sigma$ is given by figure 15, where we plot the relative error as a function of the number of averages for different electron densities. This result (figure 15) shows that it hardly makes any difference going from a density of 20 electrons per pixel (charge density ≈ 100 μC/cm²) to 200 electrons per pixel (charger density ≈ 1000 μC/cm²). The ex-

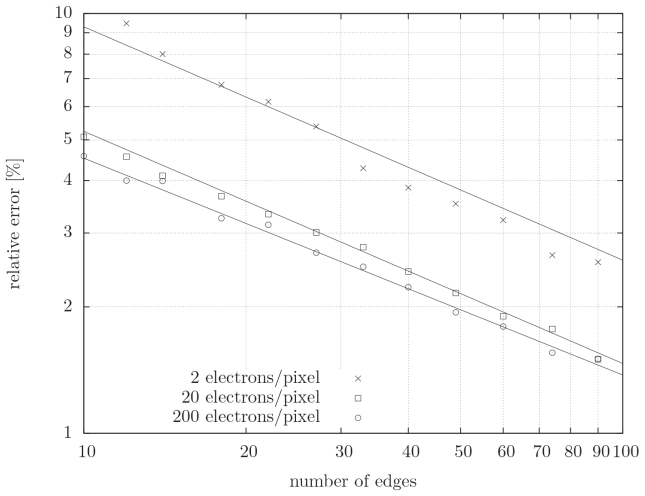


*Figure 15. Relative error in LER σ estimation when simulating different electron densities.*

planation is as follows. We identify that the relative error has two contributions: (1) image noise and (2) variation because of limited edge length. This can also be seen by integrating the Palasantzas model given by equation 10,

$$\sigma^2_{\mathrm{w/noise}} = \sigma^2_{\mathrm{w/o\ noise}} + \sigma^2_n \qquad (11)$$

The relative error is then determined as,

$$\mathrm{error}\left(\sigma^2_{\mathrm{w/noise}}\right) = \mathrm{error}\left(\sigma^2_{\mathrm{w/o\ noise}}\right) + \mathrm{error}\left(\sigma^2_n\right) \qquad (12)$$

In the simulation with an average density of 2 electrons per pixel, both terms in equation 12 contribute to the total error. The error in the noise contribution (second term in equation 12) decreases as we increase the electron density per pixel. In that case, the total relative error is primarily determined by the variation caused by limited edge length (first term in equation 12). In figure 15 we see that this already occurs at an averaged density of 20 electrons per pixel.

## 4. Conclusion

The off-line determination of LER in top-down SEM image requires low-noise images. This means that we need many electrons (higher dose) or we filter the image before edge detection. By increasing the dose we run the risk of shrinkage. The problem with a filter is that characteristics of the filter leak into the PSD. This complicates the determination of LER.

We tried a different method by fitting the profile signal of the SEM against the unfiltered images. The profile signal is obtained by integrating an experimental top-down SEM images of lines. With this method it is possible to detect the edge displacements in very noisy images without using a filter.

In a simulation study we discovered that LER can still be estimated from very noisy images with only about 2 electrons per pixel on average (charge density ≈ 10 μC/cm²). The PSDs of figure 11 are averaged over many lines. However, even a single image as figure 9, produces an estimation for LER with a relative error of only 10%. With the right analysis it is possible to get LER with reasonable accuracy at amazingly low dose.

*This work is supported by NanoNextNL, a micro and nanotechnology program of the Dutch Government and 130 partners.*

## Bibliography

[1] Yamaguchi, A., "Characterization of line-edge roughness in resist patterns and estimations of its effect on device performance," **Proceedings of SPIE 5038,** 689–698 (2003).

[2] Lee, J., Shin, J., Kim, H., Woo, S., Cho, H., Han,W., and Moon, J., "Effect of line-edge roughness (LER) and line-width roughness (LWR) on sub-100-nm device performance," **Proceedings of SPIE 5376**, 426–433 (May 2004).

[3] Gustin, C., Leunissen, L., Mercha, A., Decoutere, S., and Lorusso, G., "Impact of line width roughness on the matching performances of next-generation devices," **Thin Solid Films 516,** 3690–3696 (Apr. 2008).

[4] Patsis, G. P., Constantoudis, V., Tserepi, A., Gogolides, E., and Grozev, G., "Quantification of line-edge roughness of photoresists. I. A comparison between off-line and on-line analysis of top-down scanning electron microscopy images," **Journal of Vacuum Science & Technology B: Microelectronics and Nanometer Structures 21(3),** 1008 (2003).

[5] Yamaguchi, A., Steffen, R., Kawada, H., and Iizumi, T., "Bias-Free Measurement of LER/LWR with Low Damage by CD-SEM," **Proceedings of SPIE 6152,** 61522D–61522D–8 (Mar. 2006).

[6] Yamaguchi, A., Steffen, R., Yamamoto, J., Kawada, H., and Iizumi, T., "Single-shot method for bias-free LER/LWR evaluation with little damage," **Microelectronic Engineering 84,** 1779–1782 (May 2007).

[7] Azarnouche, L., Pargon, E., Menguelti, K., Fouchier, M., Fuard, D., Gouraud, P., Verove, C., and Joubert, O., "Unbiased line width roughness measurements with critical dimension scanning electron microscopy and critical dimension atomic force microscopy," **Journal of Applied Physics 111(8),** 084318 (2012).

[8] Hiraiwa, A. and Nishida, A., "Discrete power spectrum of line width roughness," **Journal of Applied Physics 106(7),** 074905 (2009).

[9] Mack, C. A., "Systematic errors in the measurement of power spectral density," J**ournal of Micro/Nanolithography, MEMS, and MOEMS 12,** 033016 (Sept. 2013).

[10] Ohashi, T., Sekiguchi, T., Yamaguchi, A., Tanaka, J., and Kawada, H., "Precise measurement of photoresist cross-sectional shape change caused by SEM-induced shrinkage," **Proceedings of SPIE 8681,** 86810K–86810K–12 (Apr. 2013).

[11] Yamaguchi, A. and Yamamoto, J., "Influence of Image Processing on Line-Edge Roughness in CD-SEM Measurement," **Proceedings of SPIE 6922,** 692221–692221–8 (Mar. 2008).

[12] Coleman, T. F. and Li, Y., "An Interior Trust Region Approach for Nonlinear Minimization Subject to Bounds," **SIAM Journal on Optimization 6,** 418–445 (May 1996).

[13] Palasantzas, G., "Roughness spectrum and surface width of self-affine fractal surfaces via the K-correlation model," **Physical Review B 48(19)**, 472–478 (1993).

[14] Mack, C. A., "Generating random rough edges, surfaces, and volumes.," **Applied Optics 52**, 1472–1480 (Mar. 2013).

BACUS N • E • W • S

## Sponsorship Opportunities

**Sign up now for the best sponsorship opportunities**

**Photomask 2014 —**
**Contact:** Lara Miles, Tel: +1 360 676 3290; laram@spie.org

**Advanced Lithography 2014 —**
**Contact:** Teresa Roles-Meier, Tel: +1 360 676 3290; teresar@spie.org

## Advertise in the BACUS News!

**The BACUS Newsletter is the premier publication serving the photomask industry. For information on how to advertise, contact:**

Lara Miles
Tel: +1 360 676 3290
laram@spie.org

## BACUS Corporate Members

Acuphase Inc.
American Coating Technologies LLC
AMETEK Precitech, Inc.
Berliner Glas KGaA Herbert Kubatz GmbH & Co.
FUJIFILM Electronic Materials U.S.A., Inc.
Gudeng Precision Industrial Co., Ltd.
Halocarbon Products
HamaTech APE GmbH & Co. KG
Hitachi High Technologies America, Inc.
JEOL USA Inc.
Mentor Graphics Corp.
Molecular Imprints, Inc.
Panavision Federal Systems, LLC
Profilocolore Srl
Raytheon ELCAN Optical Technologies
XYALIS

# Industry Briefs

## eBeam Initiative Announces Key Educational Themes for Photomask and Lithography Community for 2014

### PRNewswire

The eBeam Initiative, a forum dedicated to the education and promotion of new semiconductor manufacturing approaches based on electron beam (eBeam) technologies, today announced the top educational themes that it will highlight in 2014. These themes, which were identified based on member company feedback to the Initiative's most recent annual survey completed late last year, include: the growing risks associated with mask hotspots; new developments in multibeam solutions for both maskless and mask-based lithography; and new developments in general purpose graphics processing unit (GPGPU) solutions for simulation-intensive electronic design automation (EDA) applications. Mask hotspots, which are wafer-level production issues that occur when the shapes specified by optical proximity correction (OPC) are not faithfully reproduced on the mask, are of particular concern as the semiconductor industry migrates from the 28-nm node to the 20-nm node and beyond. As part of its educational efforts, the eBeam Initiative commissioned a white paper on the causes of mask hotspots, how they are different from lithography (wafer) hotspots, and solutions to address mask hotspots before they impact mask yields and cycle times, as well as wafer yields.

"eBeam technology provides a crucial link in every semiconductor design to manufacturing chain, regardless of which advanced lithography approach is being considered. After more than five years, the eBeam Initiative continues to serve a vital role in providing a forum for the mask and lithography community to explore new challenges that can be solved by eBeam based solutions," stated Aki Fujimura, CEO of D2S, the managing company sponsor of the eBeam Initiative. "Many of our members have indicated that mask hotspots are now an increasingly important issue that the industry must come together to address, making this a natural theme for the eBeam Initiative this year. Better mask making leads to better wafer making. By working together to solve the mask hotspot issue, we can enable more complex shapes to be reliably manufactured on the mask, which then addresses the lithography hotspot problem through better masks."

## Significant Progress Achieved in AIMS™ EUV Project

### Business Wire

The AIMS™ EUV platform represents an essential tool for the development and manufacturing of defect-free EUVL masks supporting the 16 nm half-pitch (HP) technology node requirements with extendibility to the 11 nm HP node. Consequently the development of this tool is part of the EUVL Mask Infrastructure (EMI) Consortium activities. SEMATECH launched EMI in 2010 to address key infrastructure gaps for EUV in the area of mask metrology, by funding development of critical metrology tools. "The AIMS™ EUV tool will be one of the most precise optical instruments fabricated for the semiconductor industry, and the EMI members are pleased to see our collaboration facilitate this technical accomplishment. With first images now available ZEISS is showing significant progress in building a production ready tool. Mask defectivity remains a key challenge to EUV readiness and it is exciting to see AIMS™ continue its journey towards realization," comments Michael Goldstein, EMI Program Manager & Sr. Principal Physicist, Intel assignee at SEMATECH.

The resolution of the system is already excellent and achieves the specification of the AIMS™ EUV system. The first images were taken on 64nm mask structures, corresponding to 16nm half-pitch at wafer level. In the course of the year the first customer masks will be measured on the system.

In parallel the preparations for the complementary AIMS™ EUV infrastructure is ongoing. Beginning in 2013 the first AIMS™ EUV Field Service Engineers were trained for installing and servicing the systems in the field.

# Join the premier professional organization for mask makers and mask users!

## About the BACUS Group

Founded in 1980 by a group of chrome blank users wanting a single voice to interact with suppliers, BACUS has grown to become the largest and most widely known forum for the exchange of technical information of interest to photomask and reticle makers. BACUS joined SPIE in January of 1991 to expand the exchange of information with mask makers around the world.

The group sponsors an informative monthly meeting and newsletter, BACUS News. The BACUS annual Photomask Technology Symposium covers photomask technology, photomask processes, lithography, materials and resists, phase shift masks, inspection and repair, metrology, and quality and manufacturing management.

### Individual Membership Benefits include:

- Subscription to BACUS News (monthly)
- Eligibility to hold office on BACUS Steering Committee

**www.spie.org/bacushome**

### Corporate Membership Benefits include:

- 3-10 Voting Members in the SPIE General Membership, depending on tier level
- Subscription to BACUS News (monthly)
- One online SPIE Journal Subscription
- Listed as a Corporate Member in the BACUS Monthly Newsletter

**www.spie.org/bacushome**

## Calendar

### 2014

**SPIE Photomask Technology**
*Co-located with*
**SPIE Scanning Microscopies**
16-18 September 2014
Monterey Marriott and
Monterey Conference Center
Monterey, California, USA
**www.spie.org/pm**

**SPIE Scanning Microscopies**
*Co-located with*
**SPIE Photomask Technology**
16-18 September 2014
Monterey Marriott and
Monterey Conference Center
Monterey, California, USA
**www.spie.org/sg**

### 2015

**SPIE Advanced Lithography**
22-26 February 2015
San Jose Convention Center
and San Jose Marriott
San Jose, California, USA
**www.spie.org/al**

SPIE is the international society for optics and photonics, a not-for-profit organization founded in 1955 to advance light-based technologies. The Society serves nearly 225,000 constituents from approximately 150 countries, offering conferences, continuing education, books, journals, and a digital library in support of interdisciplinary information exchange, professional growth, and patent precedent. SPIE provided over $3.2 million in support of education and outreach programs in 2013.

**SPIE.**
*International Headquarters*
P.O. Box 10, Bellingham, WA 98227-0010 USA
Tel: +1 360 676 3290
Fax: +1 360 647 1445
help@spie.org • www.SPIE.org

*Shipping Address*
1000 20th St., Bellingham, WA 98225-6705 USA

**Managed by SPIE Europe**
2 Alexandra Gate, Ffordd Pengam, Cardiff,
CF24 2SA, UK
Tel: +44 29 2089 4747
Fax: +44 29 2089 4750
spieeurope@spieeurope.org • www.spieeurope.org

You are invited to submit events of interest for this calendar. Please send to lindad@spie.org; alternatively, email or fax to SPIE.